ScienSage

Journal of Advanced Scientific Research

Available online through http://www.sciensage.info

ISSN
0976-9595
Research Article

INFLUENCE OF COBALT DOPING ON ROOM TEMPERATURE AMMONIA SENSING PROPERTIES OF WO_3 NANOPARTICLES GROWN BY FACILE PRECIPITATION METHOD

Duraisami Melaiyur Sankarraman[1], Benny Anburaj Durairaj[2], Parasuraman Krishnamachari*[1]

[1]*PG & Research Department of Physics, Poompuhar College (Autonomous) (Affiliated to Bharathidasan University, Tiruchirappalli), Melaiyur, Tamilnadu, India*

[2]*PG and Research Department of Physics, D. G. Govt. Arts College (Affiliated to Bharathidasan University, Tiruchirappalli), Mayiladuthurai, Tamilnadu, India*

**Corresponding author: resphy21@gmail.com*

ABSTRACT

Monoclinic cobalt (Co) doped tungsten trioxide (WO_3) nanoparticles were prepared by facile precipitation process, and are successfully used as prominent sensing material for room temperature ammonia (NH_3) gas detection. XRD, SEM, XPS and PL studies were employed to analyze the structural, morphological, surface chemistry and optical properties of the prepared samples, respectively. The gas sensing measurements disclose that, the sensor fabricated based on Co doped WO_3 nanoparticles exhibit superior selectivity and sensitivity towards NH_3 gas (S=1692 for 200 ppm, room temperature) with quick response and recovery times of 53 s and 109 s, respectively.

Keywords: Cobalt doping, WO_3, Ammonia sensor, Precipitation, BET studies.

1. INTRODUCTION

As a result of modern industrialization, various pollutants are exposed and degrade the quality of air. To address this issue, many investigations on nanotechnology have been carried out to monitor such lethal exposures. It is worth mentioning that, WO_3 is one of the most attractive nanomaterials owing to their vast technological applications in various fields such as gas sensing [1], elctrochromism [2], optoelectronics [3], photoelectro-chemical water splitting [4] and photocatalysis [5]. NH_3 is one such major air pollutant and its higher concentration level in the environment causes deleterious health effects such as irritation of eyes and throat, and even damages the lungs [6, 7]. Moreover, detection of NH_3 at its trace level is of great interest for industries because it affects the health and performance of workers and causes corrosion of instruments [8, 9]. Therefore, an efficient and robust detection approach of ammonia exposure in real time and *in situ* is desirable.

In our previous work [10], we have prepared pure WO_3 nanoparticles via one-step precipitation technique with optimal thermal treatment (823 K) and reported their NH_3 sensing properties at room temperature. However, the contribution of pure WO_3 towards NH_3 sensing is limited to some degree. Therefore, various potential approaches like doping were employed to improve the gas sensing behaviour of WO_3 nanostructures. It is well accepted that, appropriate metal ions doping into WO_3 nanostructure is one of the favourable approaches to enhance the gas sensing properties of WO_3. For instance, Yu *et al.* [11] have prepared CuO doped WO_3 nanocubes for H_2S detection. Chaudhari *et al.* [12] have reported the hydrogen sensing properties of TiO_2:WO_3 nanocrys-tallites. Bai *et al.* [13] investigated the NO_2 sensing characteristics of WO_3-SnO_2 nanocomposites and obtained the maximum sensitivity of 186 to 200 ppm of NO_2 at 200°C. WO_3/graphene nanostructures were used as NO_2 sensor, which exhibit higher sensitivity than that of undoped WO_3 sample [14].

These nano-sensors greatly contribute in many real time applications like smart fertilizers, food inspection, nanoelectro mechanical systems, environmental moni-toring and automotive emission monitoring [15-17]. In this context, we prepare Co doped WO_3 nanoparticles and investigate their NH_3 sensing behavior at room temperature. The P-type transition metal Co is assumed to be the suitable dopant for WO_3 owing to its relatively similar ionic radius (0.72 Å for Co^{2+}) to W ions (0.62 Å for W^{6+}) [18]. Invitingly, Co doped WO_3 samples exhibited a high selective behaviour towards NH_3 gas and explored a prompt response, which is twelve times greater than that of pure one.

2. EXPERIMENTAL

2.1. Material and Methods

Sodium tungstate dihydrate ($Na_2WO_4 \cdot 2H_2O$), calcium chloride dihydrate ($CaCl_2 \cdot 2H_2O$) and cobalt chloride hexahydrate ($CoCl_2 \cdot 6H_2O$) were procured from Sigma-Aldrich and used as received. De-ionized water (DI, Millipore, USA) was used as solvent in experimental solutions and Conc. nitric acid (HNO_3, Emplura, India) acted as precipitation medium. The precipitation procedure was carried out to prepare pure and Co doped WO_3 nanoparticles as demonstrated in our previous study [10].

2.2. Synthesis of pure WO_3 nanoparticles

In a typical synthesis, 1.2 mM of $Na_2WO_4 \cdot 2H_2O$ and 2 mM of $CaCl_2 \cdot 2H_2O$ were obtained using 100 ml of de-ionized water and are considered as precursor. These solutions were mixed well (~900 rpm) using a magnetic stirrer for ¾ h. Thereafter a white precipitate ($CaWO_4$) was obtained and washed several times with ethanol, acetone and distilled water. Then the precipitate was heated using a hot air oven at 60°C for 16 h, subsequently the substance was soaked in 50 ml of conc. HNO_3 for 48 h. After the completion of soaking process, the substance was filtered and cleansed many times with ethanol, acetone and distilled water. At last, the substance was placed in muffle furnace and thermally treated at 823 K for 2 h resulting in pure WO_3 nanoparticles.

2.3. Preparation of Co doped WO_3 nanoparticles

For the synthesis of Co doped WO_3 nanoparticles, 0.01 M of 100 ml $CoCl_2 \cdot 6H_2O$ aqueous solution was added in to the 0.99 M of 100 ml precipitation precursor ($CaWO_4$) solution. These solutions were transferred in to a beaker and stirred vigorously for 45 minutes. Thereafter, the settled substance was filtered, washed, dried and soaked in conc. HNO_3 as described earlier in section 2.2. Then the precipitate was calcined at 823 K to acquire Co doped WO_3 nanoparticles. The same procedure was adopted to synthesis 3 mol% and 5 mol% of Co doped WO_3 samples. The WO_3 nanoparticles prepared using 0 mol.%, 1 mol.%, 3 mol.%, and 5 mol.% of Co addition were denoted as WC0, WC1, WC3 and WC5 respectively. The concentration of Co dopant was determined using molarity relation as given in Eq. (1).

Weight= (Molarity x Molarity weight x Volume)/ 1000 1

2.4. Characterization techniques

The XRD patterns obtained from Panalytical Xpert-pro Diffractometer was used to analyze the crystal structure of the prepared samples. The SEM (ZEISS-SEM) and TEM (TEM-Hitachi H-9500) images unfold the information about the surface morphology of the synthesized samples. To disclose the elemental composition of the synthesized nanoparticles, EDAX (Bruker) analysis was employed. FTIR (Perkin-Elmer Spectrum Two, USA) and XPS (Thermo Fisher Scientific Inc., K Alpha, USA) spectra were employed to determine the vibrational modes and surface chemistry of the samples. The presence of defect states in the samples were identified through PL (Varian Cary Eclipse, USA) investigations. Brunauer-Emmett-Teller (BET) analysis was employed to estimate the surface area of the samples (Nova 3200, Quantachrome Instrument Corporation, USA). The samples were outgassed at 150°C for 3 h prior to the BET analysis.

2.5. Sensor design and testing

A customized gas sensing arrangement was used to evaluate the sensing characteristics of the synthesized samples as explained in our previous work [10]. For designing a sensing element the samples were mixed with certain amount of isopropyl alcohol (IPA), then dropcasted on a glass plate (1.5 cm x 1 cm). The glass substrate is connected to a power source which provides a D.C. potential of 10 V through a pair of copper electrodes. All the room temperature gas sensing properties of the samples have been measured using an evaporation chamber of 1 L with a computer controlled high resistance Keithley electrometer (6517B, USA). The sensing response towards different target gases was calculated using the relation given in Eq. (2).

$$S=\frac{R_a}{R_g} \quad (Ra >> Rg) \qquad .....2$$

Where R_a and R_g are the sensor resistances in air and target gas, respectively.

3. RESULTS AND DISCUSSION

3.1. Surface morphology, crystal structure and elemental analysis

Fig. 1 (a-d) depicts the SEM images of the prepared nanoparticles. Tightly packed cluster like morphology has been observed for WC0 sample. The post calcination (823 K) treatment of tungstite compound can eliminate the internal H_2O molecules and W=O permits for the layers to join through the oxygen atoms to stack together resulting in closely assembled nanostructures [19].

Randomly aggregated with spherical nanogranular morphology of Co doped WO_3 samples was obtained and the grains were distributed homogeneously throughout the surface. Co doping led to crystal defects in the host lattice which may suppress the grain growth of nanoparticles. TEM images of WC0 and WC3 samples were displayed in fig. 2 (a, b); as we can see all the samples were composed of nearly spherical nanometer size aggregates with a good dispersibility. It is also observed from TEM studies that the particle size was reduced with the increase of Co dopant concentration. The polycrystalline nature of the WC0 and WC3 samples is confirmed by SAED diffraction patterns as shown in inset of fig. 2 (a, b). XRD patterns of the synthesized samples were displayed in Fig. 3. Three major diffraction peaks (002), (020) and (200) were obtained in all samples, and the preferential growth was observed along (002) plane. Moreover, all the observed peaks were matched well with the JCPDS card #043-1035, which confirms the monoclinic crystal structure of the prepared nanoparticles.

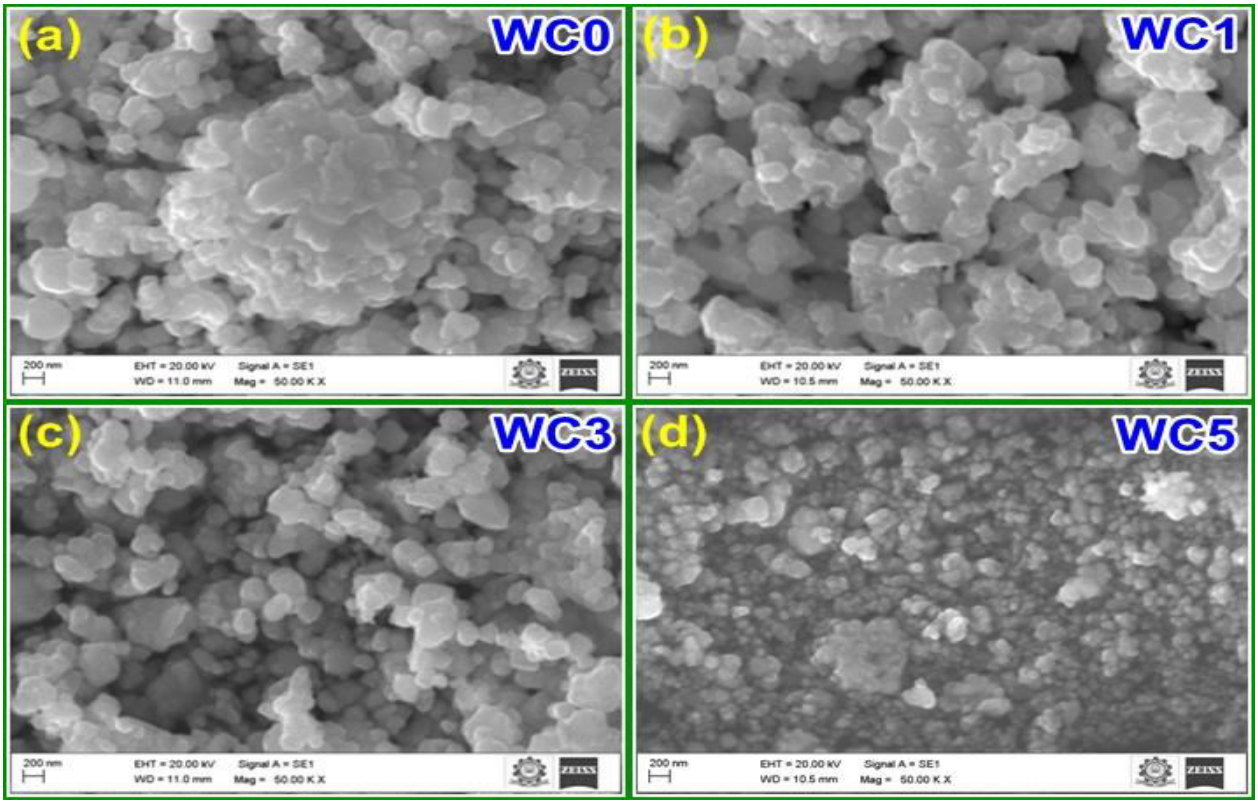

Fig. 1: SEM images of (a) pure and (b-d) Co doped WO_3 nanoparticles

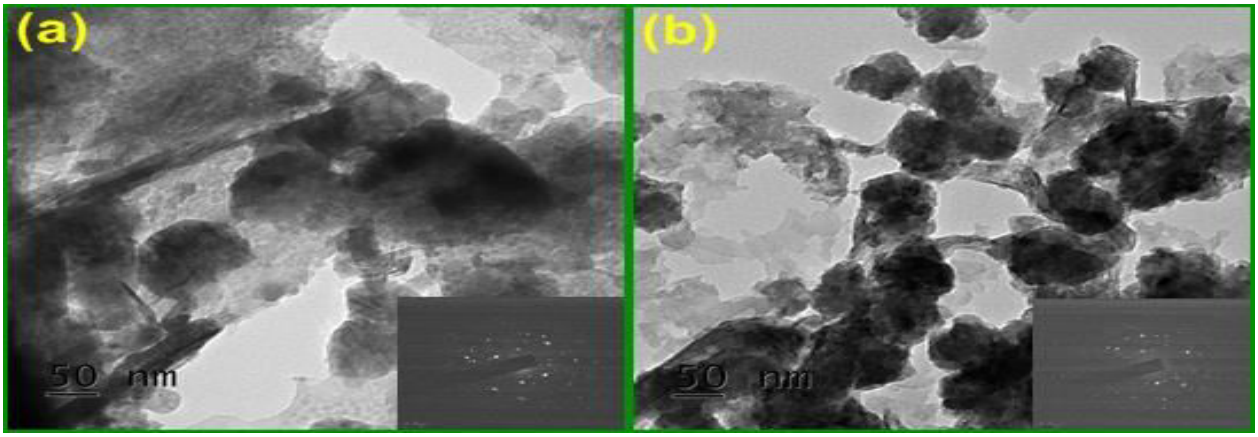

Fig. 2: TEM images of (a) WC0 (b) WC3 and (inset) SAED diffraction patterns

Invitingly, no additional peaks related to Co or any impurities were found suggesting that the successful incorporation of Co ions in to the host lattice. The mean crystallite size of the samples can be determined using Debye-Scherrer formula as given in Eq. (3).

Mean crystallite size (D) = $K\lambda / \beta\cos\theta$ --- (3)

Where K = Scherrer constant, λ = wavelength (1.5406 Å), β = full width at half–maximum and θ = Bragg angle. After introducing Co dopants the intensity of XRD peaks were diminished further and the mean crystallite size was observed to be decrease from 36.02 to 33.63 nm as displayed in table 1. This decreasing trend may be due to the introduction of Co dopants, which may cause lattice distortion and more strain in the host material.

EDAX spectra were employed to examine the elemental composition of the synthesized nanoparticles as depicted in Fig. 4. It is observed from fig. 4 (a) the WC0 sample contains W and O elements only, which indicates the formation of WO_3 without any contaminants. Moreover, the pattern discloses that the prepared WO_3 sample has a composition of W-12.37 at-% and O-87.63 at-%. Fig. 4 (b) shows the EDAX spectrum of WC3 nanoparticles, which confirms the incorporation of Co atom with the host (WO_3) sample.

It also indicates that, the WN3 sample mainly consists of W, O, and Co elements with a composition of 10.81 at -%, 86.62 at-% and 2.57 at-% respectively. These results found evidence for the formation of Co doped WO_3 nanoparticles.

Table 1: Results obtained from XRD studies

Sample	2θ (002)	FWHM (deg.)	Crystallite size (nm)
WC0	23.0231	0.22498	36.02
WC1	23.1730	0.22665	35.76
WC3	23.2731	0.23687	34.23
WC5	23.3731	0.24114	33.63

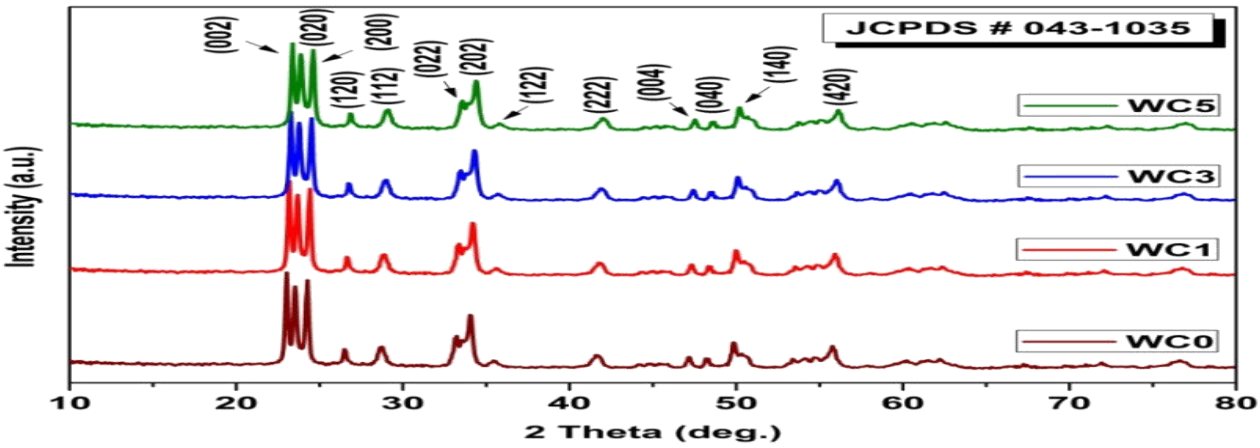

Fig. 3: XRD patterns of the prepared samples

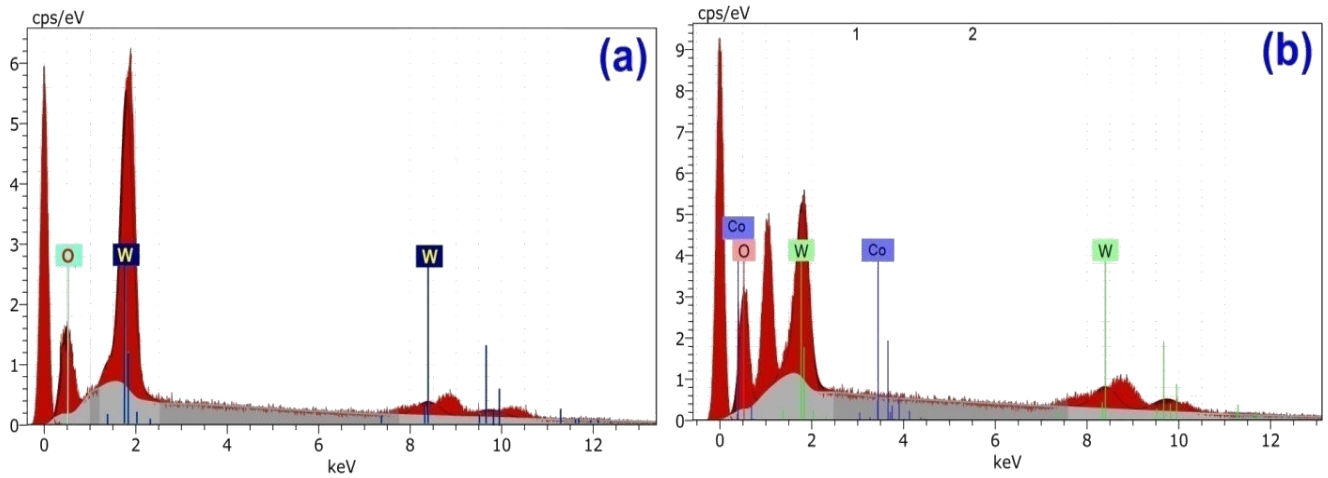

Fig. 4: EDAX spectra of (a) WC0 and (b) WC3 samples

3.2. FTIR studies

FTIR spectra of pure and Co doped WO_3 samples were displayed in fig. 5. The broad bands found at 550 to 1050 cm^{-1} is associated with the O-W-O stretching vibrational mode [20]. The bending modes of O-H groups were located at 1385 cm^{-1} and 1619 cm^{-1} [21]. Another broad band cited at 3300-3600 cm^{-1} is linked with the stretching modes of O-H groups [20, 21]. These vibrational peaks were slightly shifted to higher wave number as a consequence of Co doping. It is also observed that, there is no additional peak related to Co or any other impurities have been found. Therefore, it is evident from FTIR spectra that the Co ions were successfully doped in to the WO_3 crystal structure.

3.3. XPS studies

To study the surface elements and their corresponding ionic states, XPS analysis was employed as shown in Fig. 6. The XPS survey scan spectra of pure and Co doped WO_3 samples exhibit that all the significant peaks could be attributed to W and O elements as depicted in Fig. 6 (a). In addition, an impurity related peak is observed in WC3 sample, which could be assigned to Co 2p (encircled). Fig. 6 (b) shows the XPS core level W4f spectra indicating the appearance of two characteristic peaks related to $W4f_{7/2}$ and $W4f_{5/2}$, which demonstrates that the W elements are exist in the sample with W^{6+} valence state [22]. Moreover, the W4f peaks of WC3 sample were slightly shifted towards lower binding energy, which may be due to the effect of Co addition.

The core level XPS spectrum of Co 2p for WC3 sample showing two peaks related to Co $2p_{1/2}$ and Co $2p_{3/2}$ as shown in fig. 6 (c). This result explored that Co ions with ionic state of +2 were effectively doped with WO_3 host material [20]. Fig. 6 (d) exhibits the O1s spectra of WC0 and WC3 nanoparticles. The O1s spectra have been deconvoluted in to three peaks such as lattice oxygen species (O_L), oxygen vacancies (O_V) and chemisorbed oxygen species (O_C). These peaks were slightly displaced to lower binding energy suggesting the defective nature of the prepared nanoparticles [23].

3.4. PL spectra investigations

PL spectra of pure and Co doped WO_3 samples were shown in fig. 7. The peak observed at 412 nm is usually assigned to the recombination of free excitons and is identified as near band edge emission (NBE). The peak cited at 445 nm belongs to the rapid electron hole pair separation [24]. The blue emission peak is found at 490 nm and is designated to oxygen vacancies associated with interstitial defects in the band gap for its electron transition [24]. The particle size and morphology play crucial role in the variation of PL intensities of the synthesized samples.

When introducing Co dopants, the NBE and the defects related peaks were decreased significantly. This lower PL intensity of Co doped nanoparticles may imply the lower recombination rate of photo generated electrons and holes. This phenomenon may be due to higher defect densities under visible light irradiation. These defects can significantly improve the gas sensing properties of the synthesized nanoparticles. Similar observations have been reported in the existing literature [25].

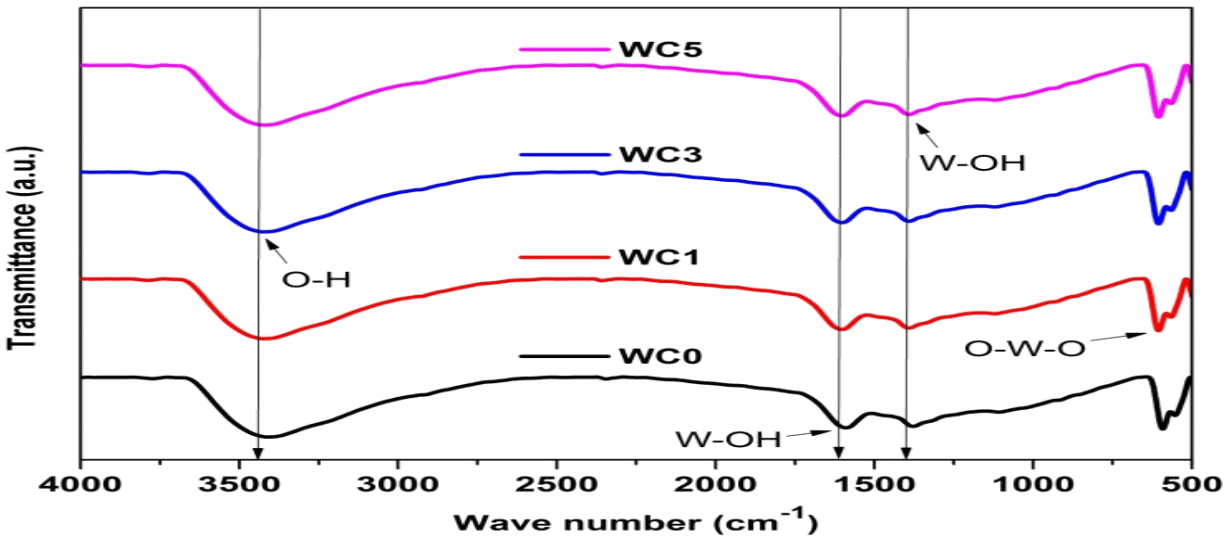

Fig. 5: FTIR spectra of pure and Co doped WO_3 samples

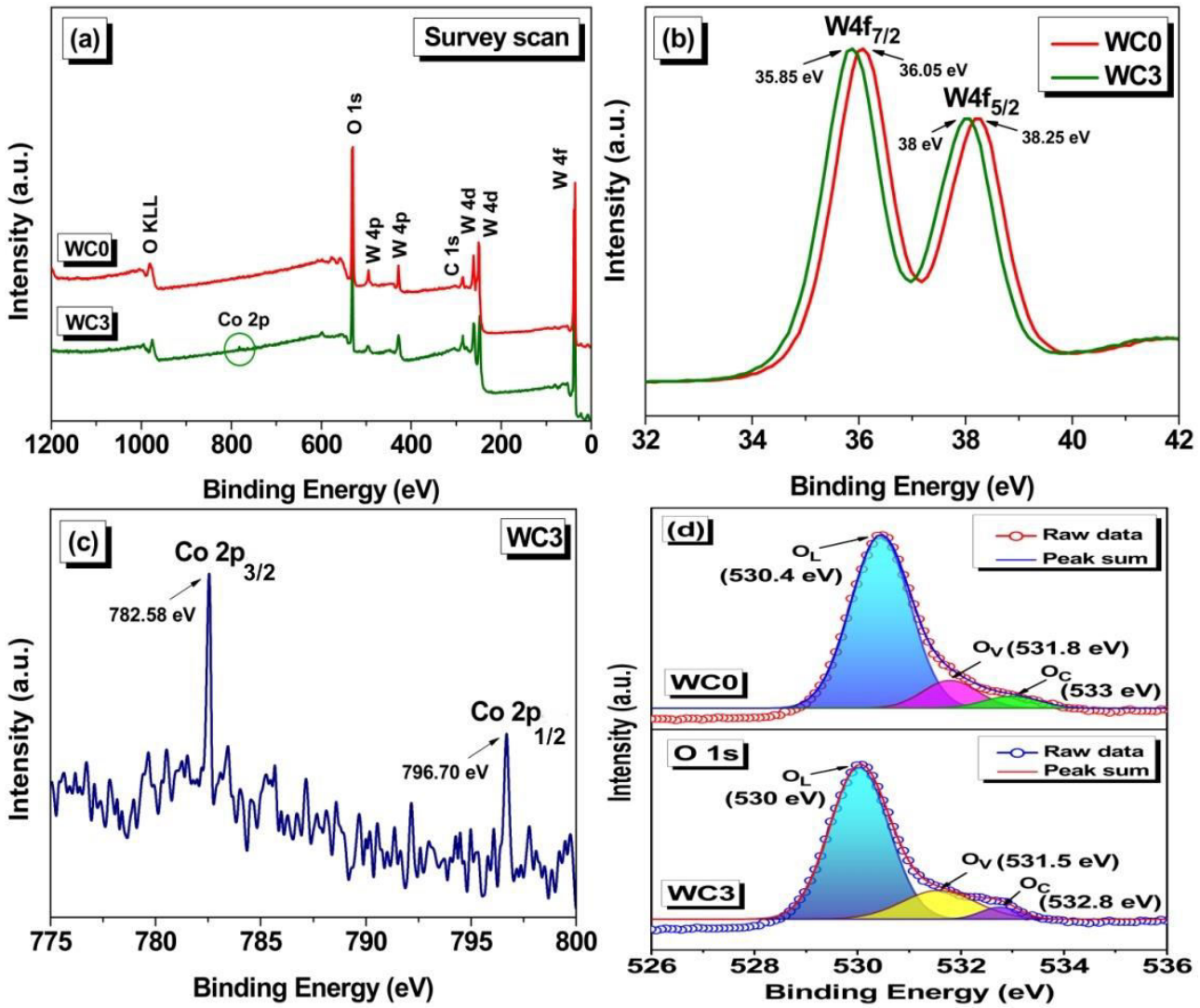

Fig. 6: (a) Survey scan spectra of WC0 and WC3 nanoparticles (b) W4f spectra (c) Co 2p core level XPS spectra (d) O 1s spectra of WC0 and WC3 samples.

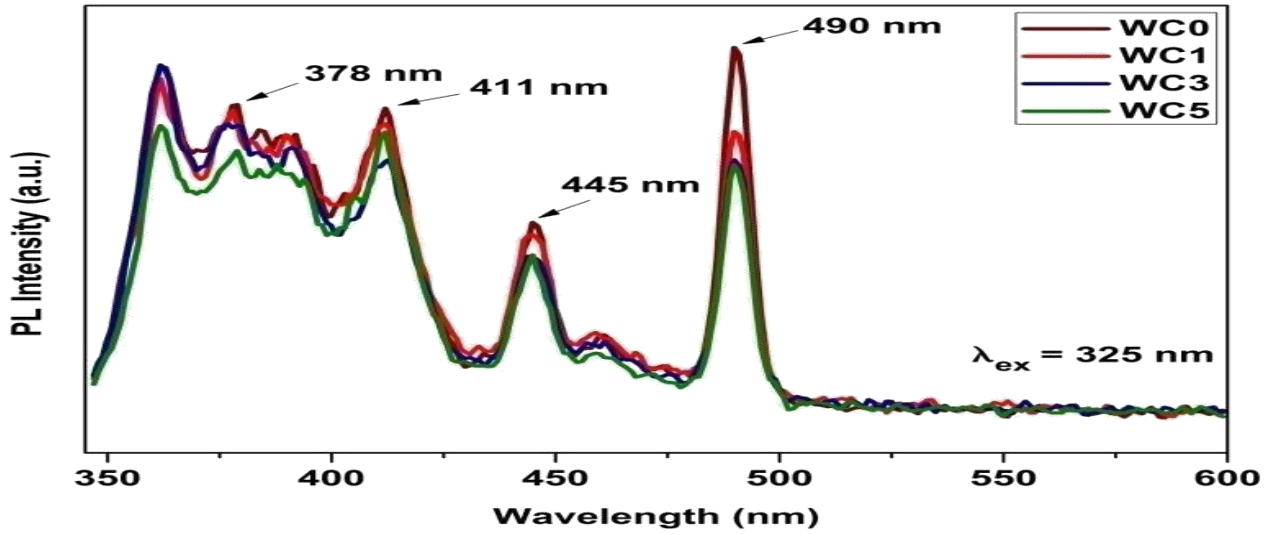

Fig. 7: Room temperature PL spectra of pure and Co doped WO_3 samples

3.5. Gas sensing characteristics

Selectivity of the synthesized nanoparticles was examined in the presence of 200 ppm of different gases such as ammonia, acetone, acetaldehyde, ethanol, formaldehyde, n-butanol, toluene and xylene at room temperature as shown in fig. 8. It is observed that all the samples exhibited high selective nature towards NH_3 gas and are little sensitive to other gases. This selective NH_3 response behaviour might be due to the following factors, (i) the lowest kinetic diameter, smaller bond dissociation enthalpy and ionization energy would make the NH_3 gas favorable for enhanced surface interactions [26], (ii) the lone pair of electrons obtained from the dissociation of H-N bond in NH_3 could have facilitated the gas-solid interaction [27, 28]. It is also inferred from selectivity studies that, the gas sensing response of WO_3 was further improved with Co doping and the maximum sensitivity was observed at WC3 sample (S=1692 for 200 ppm of NH_3) which is 12 times greater than that of WC0 (S=139 for 200 ppm of NH_3). Hence, the WC3 sample is chosen for further gas sensing investigations.

Fig. 9 (a) depicts the transient resistance response of the WC3 sensor towards 5-200 ppm of NH_3 gas at room temperature. Interestingly, the WC3 sensor exhibited superior sensitivity to NH_3 gas and its response values are 14 and 39, respectively on the exposure of 5 and 10 ppm NH_3, indicating the remarkable sensing behaviour of the sensor even at lower concentrations. The increasing trend of WC3 sensor towards various ppm level of ammonia, acetaldehyde and formaldehyde gases were displayed in fig. 9 (b). Moreover, the sensor shows a notable response to acetaldehyde (S=54, 200 ppm) and formaldehyde (S=30, 200 ppm) gases at room temperature. In order to explore the linear response trend, the WC3 sensor was investigated in the range 5-1100 ppm of NH_3 as shown fig. 10 (a). The sensor showed an excellent linear response up to 1000 ppm and reached the saturation point at 1100 ppm. This may be due to the coverage of active sites by NH_3 molecules. In addition, the lower detection limit of the sensor was found to be 1.5 ppm of NH_3. The response and recovery times of WC3 sensor for a single cycle of 200 ppm NH_3 were estimated to be 53 s and 109 s respectively, as displayed in fig. 10 (b).

Three successive measures on resistance changes were conducted to disclose the repeatable behaviour of WC3 sensor in the presence of 200 ppm NH_3 as shown in Fig. 10 (c). It can be observed that, the sensor showed a good repeatability for three consecutive evaluation cycles. The long-term stability is a significant parameter of gas sensors, which determines the accuracy of detection. Therefore, the long-term stability of WC3 sensor to 200 ppm NH_3 was measured for fifty days in the interval of ten days as depicted in fig. 10 (d). Invitingly, the WC3 sensor exhibited a remarkable sensitivity to NH_3 gas even after 50 days, and the sensing response values are just changing around 1659, indicating the excellent stable behaviour of the sensor to detect NH_3 gas at room temperature.

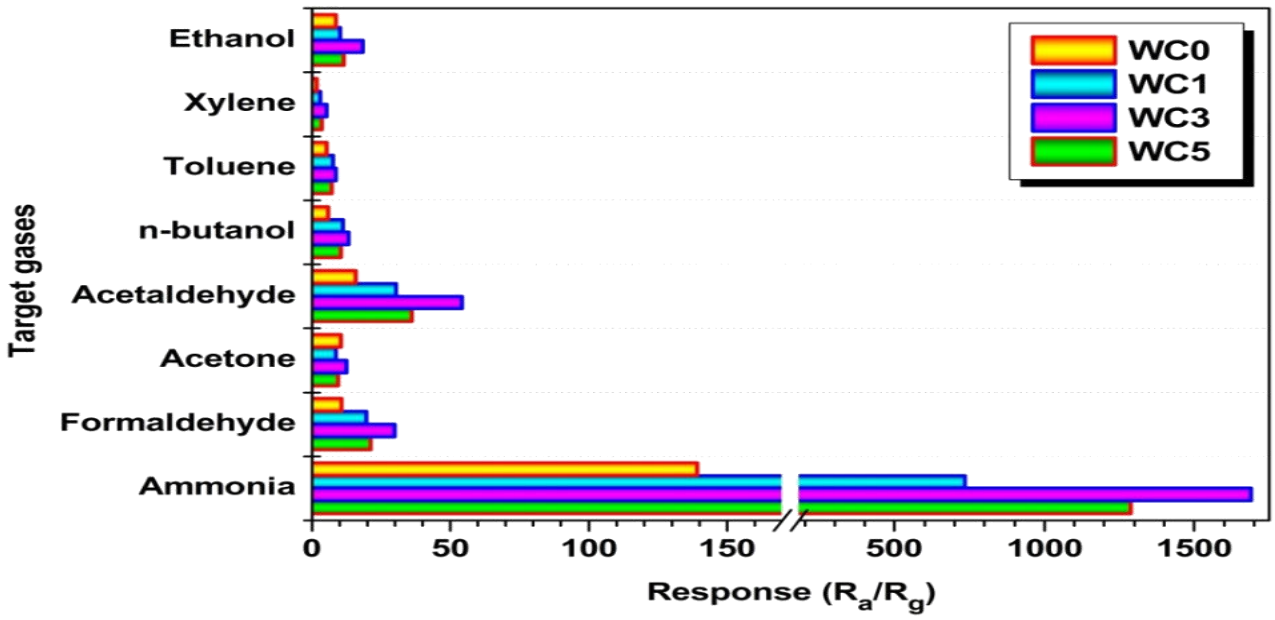

Fig. 8: Selectivity studies of WC0, WC1, WC3 and WC5 samples towards 200 ppm of different gases

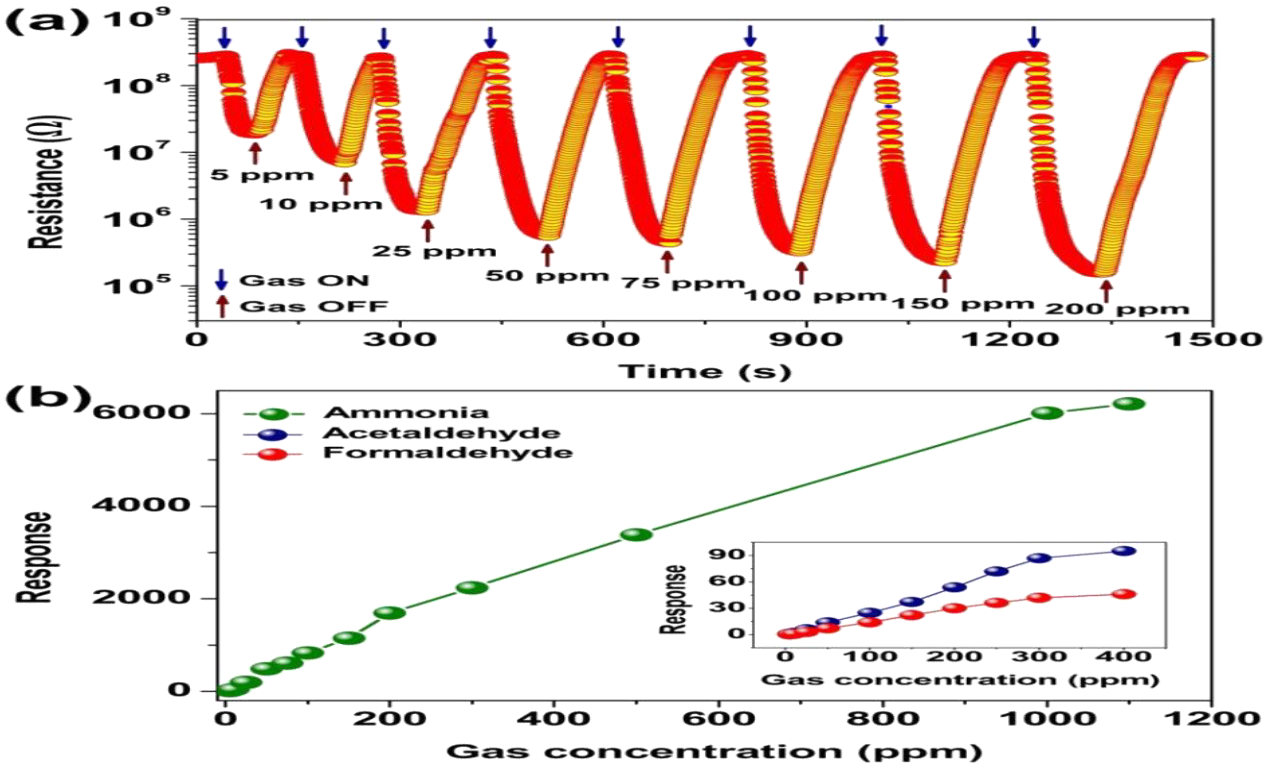

Fig. 9: (a) Transient resistance response trend of WC3 sample towards 5–200 ppm of NH_3 gas (b) Increasing trend of WC3 sample against NH_3, (inset) acetaldehyde and formaldehyde gases

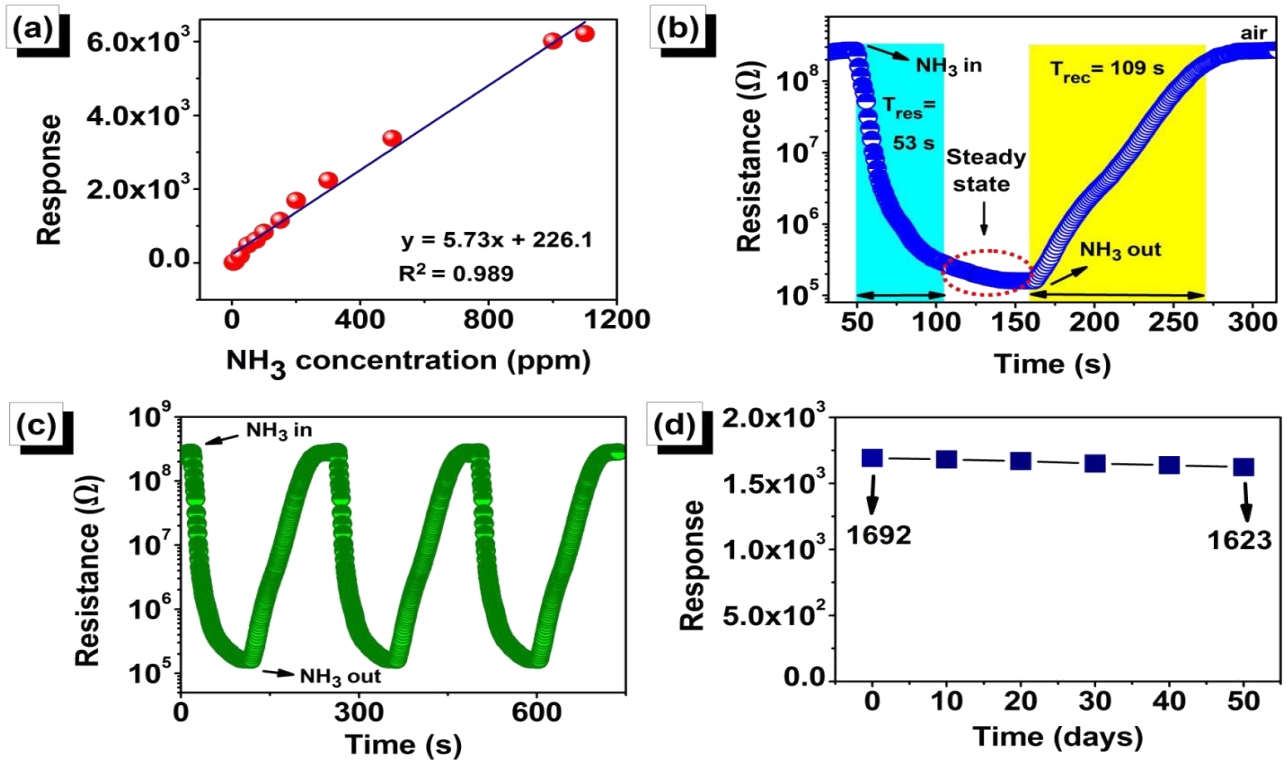

Fig. 10: (a) Linear response trend of WC3 nanoparticles against 5-1100 ppm of NH_3 gas (b) Response and recovery times of WC3 sample towards 200ppm of NH_3 (c) Repeatable behaviour (3 cycles) and (d) Stability of WC3 sample towards 200ppm of NH_3 gas

3.5.1. Sensing mechanism

As is known to all, the gas sensing mechanism of n-type semiconducting metal oxide based sensors depend on temperature and surface functionality such as reaction between chemisorbed oxygen and target gas. In the absence of NH_3 environment, n-type WO_3 nanoparticles were reacted with atmospheric oxygen species (O_2, below 100°C) and chemisorbed in the form of O_2^- on the surface by capturing the electrons from the conduction band (CB) of WO_3, which in-turn increased the width of the depletion region (Eq. (4)). The greater this space charge region, the larger will be obstruction on the movement of electrons resulting in higher resistance (R_a) of the nanoparticles [27, 28]. Under a reducing gas environment like NH_3, the target gas interacted with the surface chemisorbed O_2^- species resulting in the release of captured electrons onto the surface and are transferred back to the CB of WO_3. This led to decrease the width of depletion region and also reduced the resistance of the WO_3 thereby attaining the steady state resistance (R_g) of the material [27, 28]. The NH_3 gas sensing mechanism of WO_3 material is given in Eq. (5) [10]:

$$O_{2\,(atmosphere)} + e^-_{(WO_3\ surface)} \rightarrow O^-_{2\,(WO_3\ surface)} \quad \ldots 4$$

$$4NH_3 + 3O^-_{2\,(WO_3\ surface)} \rightarrow 2N_2 + 6H_2O + 6e^- \quad \ldots 5$$

Compared to bare WO_3, the improved sensing behaviour of Co doped WO_3 nanoparticles was probably due to several factors, which involves but is not limited to the following; (i) It is well known fact that, the P-type nature of Co^{2+} ions can provide specific adsorption sites in the WO_3 host matrix. Also, the optimal addition of Co dopant (3 mol.%) improves the surface catalytic effects like adsorption of more oxygen ions by the sensing surface, which consecutively increases the negatively charged oxygen ions that are utilized by ammonia for further oxidation. Therefore, the potential barrier of the sample may be lowered and in-turn prompt sensing reaction is ensured. (ii) The Co^{2+} metal ions were permitted to displace towards the O_2 vacancy from the coordinate center and this may develop crystal defects in the host lattice (as explained in sections 3.3 and 3.4). Due to large strain energies, these defects are designated as active sites for adsorption of NH_3 and O_2. (iii) The Co doped WO_3 nanoparticles might have enhanced the inner grain interactions with target gas and thus the width of the space charge region has been changed (decrease) significantly.

Fig. 11 depicts the specific surface area measurements of WC0 and WC3 samples using N_2 adsorption-desorption isotherms. It is observed that there is no significant difference in BET surface area between two sensors. It could be inferred that BET surface area was not a crucial factor leading to different sensing responses between WC0 and WC3 sensors. This result confirms that the addition of Co dopants had an obvious effect on improving the gas sensing properties of the WO_3 sensor. However, the sensing response of WC5 sample was decreased abruptly, which may be attributed to reduction in the number of active sites in the sample. This increasing-maximum-decreasing trend may be associated with the excess content of Co dopants which inhibits the sensing properties of the sensor [29].

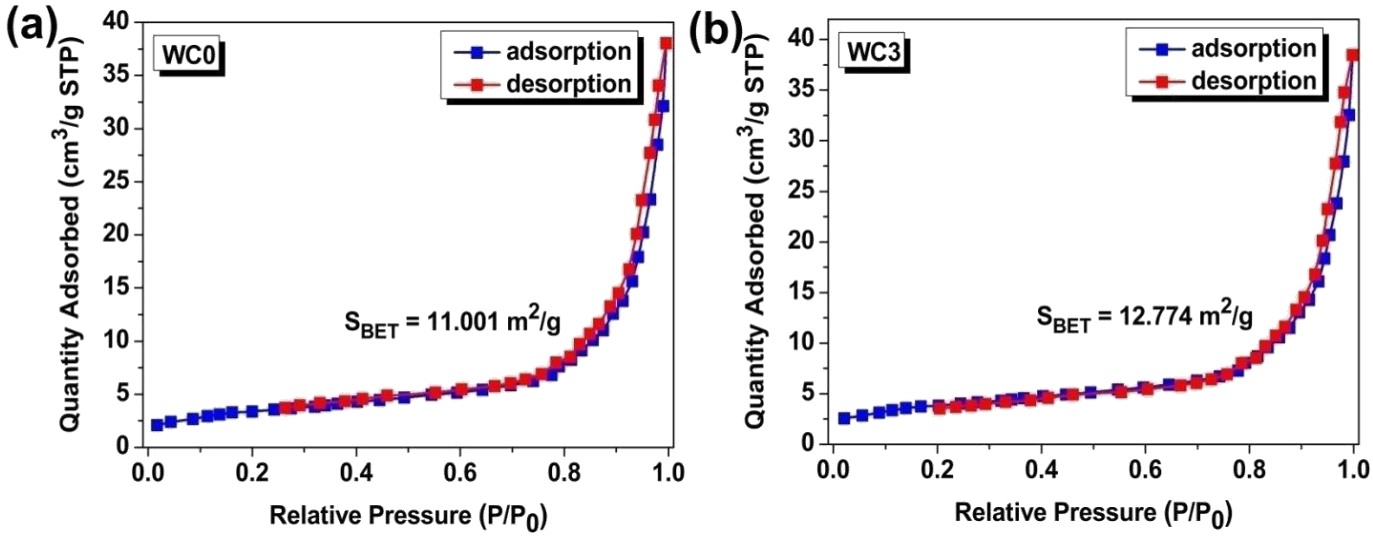

Fig. 11: N_2 adsorption / desorption isotherms of (a) WC0 and (b) WC3 samples

4. CONCLUSION

In summary, pure and Co doped WO_3 nanoparticles were successfully synthesized by simple precipitation route. Characterization studies revealed the polycrystalline monoclinic phase of the prepared samples and the average crystallite size was decreased slightly upon Co addition. The Co doping plays a crucial role in improving the gas sensing properties of the WO_3 material and the optimal performance was achieved at 3 mol. % of Co addition (WC3). The gas sensing investigations corroborate that, the WC3 sensor exhibits remarkable sensitivity (S=1692 for 200 ppm NH_3, room temperature) with faster response and recovery times of 53 s and 109 s respectively. Higher catalytic activity and large number of active sites played an important role in improving the sensing properties. Also, the WC3 sensor shows excellent figure of merits such as larger active detection range, good repeatability and long-term stability to NH_3 gas. Thus the reported sensor could be a promising candidate for monitoring NH_3 gas at room temperature. To highlight this study, NH_3 sensing performance of WC3 sensor in the present work is compared with those available reports [30-34].

Table 2: Comparison of NH_3 sensing performances of various gas sensors

Synthesis Technique	Dopant Material	Sensing Response	Concentration (ppm)	Response time (s)	Recovery time (s)	Operating Temperature (K)	Ref.
Spray pyrolysis	Cd (2 at.%)	5[b]	100	30	53	473	[30]
Spray pyrolysis	Cu (20 wt.%)	3.4[a]	50	30	14	303	[31]
Calcination (powder)	Ga (10 at.%)	2[b]	18	-	-	723	[32]
Spray pyrolysis	Na (1 M)	1.7[a]	500	-	-	673	[33]
Hydrolysis	Ag (3 mol.%)	25.1[a]	10	150	600	303	[34]
Precipitation	Co (3 mol.%)	1692[a]	200	53	109	303	This work

[a] $S=\frac{R_a}{R_g}$, [b] $S=\frac{(R_a-R_g)}{R_a}\times 100$

5. ACKNOWLEDGEMENT

One of the authors (M.S. Duraisami) gratefully acknowledge his sincere thanks to Nanosensor Lab, SASTRA Deemed to be University, Thanjavur, India for carried out gas sensing studies.

Conflict of interest

The authors declare that they have no known competing interests.

6. REFERENCES

1. Siciliano T, Tepore A, Micocci G, Serra A, Manno D, Filippo E. *Sens. Actuators B Chem*, 2008; **133 (1):**321-326.
2. Munro B, KrAmer S, Zapp P, Krug H. *J Solgel Sci Technol,* 1998;**13:**673-678.
3. Shao D, Yu, Lian J, Sawyer S. *Optical Materials*, 2014; **36(5):**1002-1005.
4. Jansi Rani B, Praveen Kumar M, Ravichandran S, Ravi G, Ganesh V, Ramesh K. Guduru. et al. *J. of Phys. and Chem. of Solids*, 2019; **134:**149-156.
5. Tahir MB, Nabi G, Khalid NR, Khan WS. *J. Inorg. Organomet Polym,* 2018; **28:**777-782.
6. Leung CM, Foo CL. *Ann. Acad. Med. Singapore*, 1992; **21 (5):**624-629.
7. Close LG, Catlin FI, Cohn AM. *Arch. Otolaryngol,* 1980; **106 (3)**:151-158.
8. Timmer B, Olthuis W, Van Den Berg A. *Sens. Actuators B Chem,* 2005; **107(2)**:666-677.
9. Malins C, Doyle A, MacCraith BD, Kvasnik F, Landl M, Simon P, et al. *J. Environ. Monit*. 1999; **1:**417-422.
10. Duraisami MS, Parasuraman K. *Nanosystems: Phys. Chem. Math,* 2020; **11(5):**578-589.
11. Yu W, Sun Y, Zhang T, Zhang K, Wang S, Chen X, et al. *Part. Part. Syst. Charact*. 2015; **33:**15-20.
12. Chaudhari GN, Bende AM, Bodade AB, Patil SS, Sapkal VS. *Sens. Actuators B Chem,* 2006; **115:**297-302.
13. Bai S, Li D, Han D, Luo R, Chen A, Chung CL. *Sens. Actuators B Chem,* 2010; **150:**749-755.
14. An X, Yu JC, Wang Y, Hu Y, Yu X, Zhang G. *J. Mater. Chem,* 2012**; 22:**8525-8531.
15. Xu K, Fu C, Gao Z, Wei F, Ying Y, Xu C, et al. *Instrum. Sci.Tech,* 2017; **46(2):**115-145.
16. Vander Wal RL, Hunter GW, Xu JC, Kulis MJ, Berger GM, Ticich TM. *Sens. Actuators B Chem*, 2009; **138:**113-119.
17. Yeganeh M, Nguyen TA. *Kenkyu J. Nanotechnol.*

Nanosci, 2019; **5:**37-44.
18. Sun S, Chang X, Li Z. *Mater. Charact,* 2012; **73:**130-136.
19. Ahmadi M, Sahoo S, Younesi R, Gaur APS, Katiyar RS, Guinel MJF. *J. Mater. Sci*, 2014; **49(17):** 5899-5909.
20. Mehmood F, Iqbal J, Jan T, Gul A, Mansoor Q, Faryal R. *Vib. Spectrosc*, 2017; **93:**78-89.
21. Delichere P, Falaras P, Froment M, Goff AHL. *Thin Solid Films*, 1988; **161:**35-46.
22. Song H, Li Y, Lou Z, Xiao M, Hu L, Ye Z, et al. *App. Catalysis B Environ,* 2015; **166:**112-120.
23. Vuong NM, Kim D, Kim H. *Sci. Rep.* 2015; **5:**1-13.
24. Lee K, Seo WS, Park JT. *J. Am. Chem. Soc.* 2003; **125:**3408-3409.
25. Zhang H, Yangb J, Lib D, Guob W, Qinb Q, Zhua L, et al. *Appl. Surf. Sci*, 2014; **305**:274-280.
26. Nayak AK, Ghosh R, Santra S, Guha PK, Pradhan D. *Nanoscale*, 2015; **7:**12460-12473.
27. Mani GK, Rayappan JBB. *Appl. Surf. Sci*, 2014; **311:**405-412.
28. Mani GK, Rayappan JBB. *Sens. Actuators B Chem,* 2013; **183:**459-466.
29. Sun Y, Chen L, Wang Y, Zhao Z, Li P, Zhang W, et al. *J Mater Sci,* 2017; **52:**1561-1572.
30. Tarwal NL, Patil AR, Harale NS, Rajgure AV, Suryavanshi SS, Bae WR, et al. *J. Alloys. Compd,* 2014; **598:**282-288.
31. Mani GK, Rayappan JBB. *J. Alloys.Compd,* 2014; **582**:414-419.
32. Vorobyeva N, Rumyantseva M, Konstantinova E, Grishina D, Gaskov A. *Procedia Eng,* 2011; **25:**296-299.
33. Mariappan R, Ponnuswamy V, Suresh R, Suresh P, Chandra Bose A, Ragavendar M. *J. Alloys. Compd,* 2014; **582**:387-391.
34. Liu H, Shen W, Chen X. *RSC Adv,* 2019; **9:**24519-24526.